ELSEVIER

Combustion and Flame 133 (2003) 75–91

Combustion and Flame

Spectral radiative effects and turbulence/radiation interaction in a non-luminous turbulent jet diffusion flame

P.J. Coelho[a,*], O.J. Teerling[a], D. Roekaerts[b]

[a]*Instituto Superior Técnico, Mechanical Engineering Department, Av. Rovisco Pais, 1049-001 Lisboa, Portugal*
[b]*Delft University of Technology, Thermal and Fluids Sciences, Department of Multi-Scale Physics, P.O. Box 5046, 2600 GA Delft, The Netherlands, Shell Research and Technology Centre, Amsterdam*

Received 10 April 2002; received in revised form 13 September 2002; accepted 12 November 2002

Abstract

A non-luminous turbulent jet diffusion flame is numerically simulated using a Reynolds stress second-order closure, the steady laminar flamelet model, and different approaches for radiative transfer. The commonly used optically thin approximation is compared with the discrete ordinates method. Calculations using the Planck mean absorption coefficient are compared with computations performed using the spectral line-based weighted-sum-of-gray-gases model. The interaction between turbulence and radiation is simulated, and its influence on the predicted results is investigated. It is shown that the discrete ordinates method and the optically thin approximation yield relatively close results for the present flame if the medium is modelled as gray using the Planck mean absorption coefficient. In both cases, the predicted fraction of radiative heat loss is significantly overestimated. However, if the spectral nature of gaseous radiation is accounted for, the computed radiation loss is closer to the experimental data. The fluctuations of the species have a minor role in the interaction between turbulence and radiation, which is mainly due to the temperature fluctuations.

Keywords: Turbulent diffusion flames; Turbulence/radiation interaction; Laminar flamelet model; Radiative heat transfer

1. Introduction

Flame radiation plays an important role in fires and in many combustion systems. Pollutant emissions are also influenced by flame radiation by means of their dependence on the temperature field. For example, the accurate prediction of NO in turbulent jet diffusion flames requires an accurate prediction of the flow/mixing field and radiation losses, as well as a detailed mechanism of NO formation and destruction. The present work is concerned with the prediction of the radiation losses from non-luminous turbulent diffusion flames.

The calculation of radiation from flames has often been based on the optically thin approximation, e.g. [1], neglecting flame absorption, particularly in the case of non-luminous flames. However, this is a crude approximation in many applications, especially if an accurate prediction of the temperature field is needed, as in the case where NO predictions are required. More accurate radiative calculations may be carried out using, for example, the zone [2], Monte Carlo [3], spherical harmonics [4], discrete transfer [5], discrete ordinates [6], and boundary element [7] methods. However, the medium has been considered as gray in most simulations. Here, the word ‘gray’ characterizes the radiation model, and not the gas radiative properties model. This means that radiative calculations are carried out using total radiative properties, no matter how these are calculated. An ad-

* Corresponding author. Tel.: +1-351-218418194; fax: +1-351-218475545.
E-mail address: coelho@navier.ist.utl.pt (P.J. Coelho).

0010-2180/03/$ – see front matter
doi:10.1016/S0010-2180(02)00542-4

vanced non-gray model may be used to compute the gas radiative properties, e.g., a narrow band model, but if it is used only to compute total radiative properties, and the radiation model uses these total radiative properties, i.e., spectral band calculations are not carried out, then we still say that the medium is treated as gray.

It is well known that gas radiation occurs in discrete bands that comprise many thousands of spectral lines. Line-by-line calculations cannot be used in practical problems because of their computational costs, but several non-gray gas radiative property models are available. A survey of these models and their coupling with the radiative transfer equation may be found in [8]. The statistical narrow band model has been used to compute the radiation intensity along lines of sight [9], and as a post-processor (uncoupled calculations) to calculate radiative wall fluxes and power in a turbulent flame inside an axisymmetrical furnace [10]. However, narrow band calculations are too computationally expensive for coupled flame structure and radiation simulations. The exponential wide band model [11] may be used in flame calculations, e.g. [12–14], but the correlation between the spectral transmissivity and the radiation intensity is generally ignored. These non-correlated calculations may yield large errors, as shown in [15]. The correlated formulation is time-consuming and difficult to couple to differential solution methods of the radiative transfer equation (RTE), such as the discrete ordinates method (DOM) [16].

The correlated k-distribution method [17], initially developed in the atmospheric radiation community, has recently received the attention of the heat transfer community [18,19]. It provides the absorption coefficient as the basic radiative property, contrary to the narrow and wide band models, and therefore may be easily applied together with any solution method of the RTE. Unfortunately, it is still quite expensive for most practical applications. The computational requirements depend on the number of bands, number of quadrature points within a band and number of absorbing gases in the mixture. In the case of 44 bands and 7 quadrature points per band, the ratio of the CPU time for the correlated k-distribution method to the CPU time for the classical weighted-sum-of-gray-gases (WSGG) model [20] with 8 coefficients is 28 for a H_2O-N_2 gas layer and 11 for a CO_2-N_2 gas layer [21]. In the case of a H_2O-CO_2-N_2 mixture, that ratio generally exceeds two orders of magnitude [22].

The WSGG model [20], initially developed to use together with the zone method, is probably the most popular method to compute the gas radiative properties. However, it has generally been used to compute the total emissivity, treating the gas as a gray medium. Only after the work of Modest [23] it has been implemented as a non-gray gas model in the RTE, and coupled with the discrete ordinates and the discrete transfer methods [10,24]. However, in the case of significant temperature gradients, the WSGG model may yield important errors, higher than 30%, as discussed in [10].

The spectral line-based weighted-sum-of-gray-gases (SLW) model developed by Denison and Webb [25] is an improved version of the WSGG model, which has emerged in the last decade as a promising alternative model able to provide high accuracy at moderate computational cost, and compatibility with any arbitrary solution method of the RTE. A closely related model, referred to as absorption distribution function model [26], differs only in the calculation of the weights. The full-spectrum correlated-k distribution [27] and the multi-scale correlated k-distribution [28] methods, recently developed by Modest and co-workers, have many similarities with the SLW model. They extend the correlated-k distribution to the entire spectrum by defining a fractional Planck function, thus combining all the advantages of the correlated k-distribution method with those of global models.

In the case of turbulent flames, there is a lot of experimental and theoretical evidence that the turbulence/radiation interaction (TRI) has a significant influence due to the temperature and species concentration fluctuations and the non-linear relationship among temperature, radiative properties and radiation intensity [29]. Despite of this, most works neglect such an interaction. At present, the most accurate way to simulate the TRI seems to be the stochastic approach, firstly employed by Jeng et al. [9]. They assumed that the flow field consists of numerous statistically independent turbulent eddies, each of them having uniform properties, which were assumed to be a single function of mixture fraction. The instantaneous mixture fraction was randomly selected according to a prescribed cumulative distribution. Temporal correlations were ignored in their model. The model was modified in [30] to account for temporal correlations of mixture fraction, and in [31] to remove the restriction of statistically independent eddies, and some minor improvements were reported in [32,33]. Chan and Pan [34] have shown that cross temporal-spatial correlations are also important. They further improved the model by including all together the mixture fraction correlations in space and time, their cross correlations, and post-correlations in space [35].

The above works were restricted to the calculation of spectral intensities along a line of sight, and were not applied to the simulation of radiative transfer in flames. Despite the promising results achieved by the

stochastic approach, it suffers from the time-consuming need to take many trials for good statistics, and may not be practical in modelling complex combustor geometries, as recognized by Hall and Vranos [36]. These authors have developed a simpler and faster semi-analytic approach, and applied their method to a turbulent CH_4-H_2 diffusion flame using the wide band model. In another approach, which avoids a detailed knowledge of two-point correlations of temperature and concentration fluctuations, the integral form of the RTE is taken and the instantaneous terms in the exponential expressions are replaced by time averaged values [37]. Such an approximation is only valid if the optical dimension of the turbulent eddies is <0.3.

Several authors have simplified the time averaged RTE by assuming that there is no correlation between temperature and concentration within each eddy. This is a consequence of assuming that the individual eddies are homogeneous, optically thin, and statistically independent. Song and Viskanta [38] have used this approach together with the spherical harmonics P1 approximation for the simulation of a natural gas fired furnace. This approach has also been used in [39] in the framework of a ray tracing method, in [40] together with the DOM, and in [41] along with the four-flux radiation model. The same approximation was recently used in [42] with the P1 and wide band models for radiative calculations and the velocity-composition joint probability density function (PDF) method [43] for flow and combustion modeling. These PDF methods for turbulent reactive flows can also be combined with the boundary element method applied to radiative heat transfer and accounting for the TRI [44].

The motivation for the present work stems from the questions raised at the International Workshop on Measurement and Computation of Turbulent Non-Premixed Flames [45] regarding the appropriateness of the optically thin assumption for the piloted flames. The large discrepancies between NO predictions made by different research groups and investigators motivated the measurement of radiative heat loss from the flames. It was found that the measured radiant fraction for the so-called flame D was 5.1% compared with predicted values of 10.5% and 12.5% using the PDF and conditional moment closure (CMC) models along with the optically thin approximation [46]. However, independent calculations based on a full joint PDF method and the same optically thin approximation [47] gave a value of 2.85% for the total radiant fraction accounting only for $x/d \leq 60$. This suggests that the measured value might be approached if the entire flame were considered. Therefore, there is a need to a more accurate treatment of radiative transfer to address this problem.

In this work, flame D is simulated using a Reynolds stress model for turbulence modeling, the steady laminar flamelet model for combustion, the DOM for radiation, the SLW model for the radiative properties of the gas, and the approach of Song and Viskanta [38] to account for the TRI. For comparison purposes, calculations have also been performed using the optically thin approximation. The main contribution of the present work is to present and apply a model for flame simulation that simultaneously accounts for flame radiation using advanced radiation and gas radiative properties models, as well as TRI. Some researchers have used the DOM or the discrete transfer method in flame simulations. Others, but very few, have treated the medium as non-gray in the radiation model. Also very few have accounted for the TRI. Here, all these features are simultaneously accounted for, and their role is investigated and compared with simpler approaches.

The influence of the spectral radiation effects and the TRI are investigated. The models are described in the next section, with emphasis on the radiative transfer calculations. Then, some computational details are provided, and the experimental configuration is described. This is followed by the presentation and discussion of the results. The main conclusions are drawn in the last section.

2. Mathematical modeling

2.1. Turbulence model

Full second moment turbulence closure was used [48]. The transport equation for the Reynolds stress was modeled after Launder, Reece, and Rodi [49] (LRR-IP model), and the transport equation for the Reynolds flux of a scalar was closed by a widely used model described by Jones [50]. Standard values were assigned to the constants of the model, with one exception: in the standard equation for the dissipation rate of turbulent kinetic energy the constant $C_{\varepsilon 1}$ is set to 1.60 to improve the prediction of the spreading rate of the jet. The computational fluid dynamics (CFD) code employed in the present work is an in-house code developed at the Delft University of Technology. It solves the density weighted averaged form of the governing equations by using the finite volume method and a non-staggered grid variable arrangement.

2.2. Combustion model

Combustion is modeled using the conserved scalar approach with a prescribed probability density function. According to this approach, in the case of

an adiabatic flow the instantaneous thermochemical state of the gaseous mixture is a function of a strictly conserved scalar variable, taken as the mixture fraction. Here, this function is obtained using the laminar flamelet concept.

The flamelet model is based on the idea that a turbulent flame may be regarded as an ensemble of flamelet structures attached to the instantaneous position of the flame surface, which is corrugated by the turbulent flow field [51]. The flamelet structure may be calculated from the solution of the flamelet equations. These equations are derived from the transport equations for species mass fractions and energy by means of a coordinate transformation. If the pressure is constant with time, and the Lewis number for all the species is equal to 1, then the flamelet equations for non-premixed combustion may be written as:

$$\rho \frac{\partial T}{\partial t} - \rho \frac{\chi}{2} \frac{\partial^2 T}{\partial Z^2} - \rho \frac{\chi}{2c_p} \frac{\partial T}{\partial Z} \frac{\partial c_p}{\partial Z} - \sum_i \left(\rho \frac{\chi}{2} \frac{c_{pi}}{c_p} \frac{\partial Y_i}{\partial Z} \frac{\partial T}{\partial Z} \right) + \frac{1}{c_p} \sum_i \dot{w}_i h_i + \frac{\nabla \cdot \mathbf{q}}{c_p} = 0 \quad (1)$$

$$\rho \frac{\partial Y_i}{\partial t} - \rho \frac{\chi}{2} \frac{\partial^2 Y_i}{\partial Z^2} - \dot{w}_i = 0 \quad (2)$$

where T is the temperature, Y_i the mass fraction of species i, ρ the density, χ the scalar dissipation rate, c_p the specific heat capacity, t the time, Z the mixture fraction, $\dot{w}$ the reaction rate, h the enthalpy, $\nabla \cdot \mathbf{q}$ the radiative source per unit volume, and the subscript i refers to the ith chemical species. Although previous work [52] has shown that the unsteady laminar flamelet model performs better than the steady model, the difference between the H_2O and CO_2 mass fractions predicted by the two models is relatively small. Because these species are responsible for most of the radiation loss, which is of primary concern in the present work, the steady flamelet model will be used here. Therefore, only the steady solution of Eqs. (1) and (2) is required. However, the time dependent terms are retained in Eqs. (1) and (2), because these equations are solved using a marching in time solution algorithm until the steady state solution is attained.

The temperature field predicted by the steady laminar flamelet model considering radiation is unrealistic, as shown in [53]. Therefore, the radiation term was omitted in the solution of the flamelet equations, and the temperature computed from Eq. (1), corresponding to adiabatic conditions, was used to calculate the density field in Eq. (2). The temperature and density fields for non-adiabatic conditions are obtained from the enthalpy, as described later. According to this approach, radiative transfer does not influence the flamelet relationships between instantaneous values of chemical composition and mixture fraction. This simplification is expected to have a minor influence for the present flame, because the total fraction of radiative heat loss is about 5%. The influence should be greater in strongly radiating flames. This expectation is confirmed by previous calculations reported in [52], which were carried out using both the steady laminar flamelet model, that neglects the influence of radiative transfer on the flamelet relationships, and the unsteady flamelet model, that accounts for it. It was found that the predictions of concentration of major species, including CO_2 and H_2O, were similar for both models, showing that this simplification is acceptable.

The scalar dissipation rate, which is a function of the mixture fraction, is an important parameter in the flamelet equations. It can be interpreted as the inverse of a characteristic diffusion time. This function may be taken from counter-flow geometry [54] as

$$\chi(Z) = \frac{a}{\pi} \exp\{-2[erfc^{-1}(2Z)]^2\} \quad (3)$$

where erfc^{-1} is the inverse of the complementary error function and a is the velocity gradient at the stagnation point. Applying Eq. (3) to stoichiometric conditions yields

$$\chi(Z) = \chi_{st} f(Z)/f(Z_{st}) \quad (4)$$

where $f(Z)$ is the exponential term on the right of Eq. (4) and the subscript st identifies stoichiometric conditions. This expression for the scalar dissipation rate is used in Eqs. (1) and (2). The scalar dissipation rate for the stoichiometric mixture, χ_{st}, is taken as a flamelet parameter, that is, the solution of the flamelet equations is a function of Z and χ_{st}.

For turbulent flows Eq. (4) must be averaged. Assuming that χ_{st} and Z are statistically independent [51] that equation may be expressed as

$$\tilde{\chi} = \tilde{\chi}_{st} \left(\int_0^1 f(Z) \tilde{P}(Z)\, dZ \right) / f(Z_{st}) \quad (5)$$

where $\tilde{P}(Z)$ is the pdf of mixture fraction. The averaged scalar dissipation rate $\tilde{\chi}$ is the sink term of the transport equation for the mixture fraction variance, $\widetilde{Z''^2}$, which is modeled by

$$\tilde{\chi} = C_x \frac{\varepsilon}{k} \widetilde{Z''^2} \quad (6)$$

C_x is a constant set equal to 2.0 [55]. The conditional mean scalar dissipation rate at $Z = Z_{st}$, $\tilde{\chi}_{st}$, calculated from Eqs. (5) and (6) can be set equal to χ_{st} in

Eq. (4) because of the inertial range invariance of scalar dissipation rates [56].

In the CFD code transport equations are solved for $\tilde{Z}$ and $\widetilde{Z''^2}$. The mean and the variance of the mixture fraction completely define the pdf, assumed to be a beta function. The Favre mean values of the mass fractions are calculated by integrating the flamelet profiles, parameterized by the local value of $\tilde{\chi}_{st}$, over the mixture fraction range

$$\tilde{Y}_i = \int_0^1 Y_i(Z, \tilde{\chi}_{st})\tilde{P}(Z)\, dZ \tag{7}$$

A transport equation for the mean enthalpy, $\tilde{h}$, is also solved in the CFD code. It may be written as

$$\frac{\partial}{\partial x_j}(\bar{\rho}\tilde{u}_j\tilde{h}) = \frac{\partial}{\partial x_j}\left(\frac{\mu}{\sigma}\frac{\partial \tilde{h}}{\partial x_j} - \bar{\rho}\widetilde{u_j h}\right) - \overline{\nabla \cdot \mathbf{q}} \tag{8}$$

where $\tilde{u}_j$ is the Favre-averaged jth velocity component, x_j is the coordinate along direction j, μ is the viscosity, and σ is the Prandtl number. The tilde identifies Favre-averaged quantities. The mean temperature field is computed from the enthalpy, as described below.

The enthalpy of the mixture is defined by

$$h = \sum_i Y_i h_i = \sum_i Y_i\left(h_i^o + \int_{T^o}^{T} c_{p,i}\, dT\right) \tag{9}$$

where Y_i is the mass fraction of species i, and h_i^o is the enthalpy of formation of the same species at the standard reference temperature T^o. The following relation holds for adiabatic conditions

$$h_{ad} = h_{ox}(1 - Z) + h_{fu}Z \tag{10}$$

where h_{ox} and h_{fu} are the enthalpies of the oxidant and fuel, respectively.

The local fraction of radiative heat loss, X_R, is defined as [57]

$$X_R = \frac{h_{ad} - h}{h_{ad} - \sum_i Y_i h_i^o} \tag{11}$$

This is a non-dimensional quantity that is defined from local values of enthalpy and species concentrations. It represents the ratio of the local energy released by radiation to the energy that would have been released if the products were cooled down to the room temperature. Eq. (11) may be rearranged as follows, showing the independent variables for clarity

$$h(Z, \chi_{st}, X_R) = X_R \sum_i Y_i(Z, \chi_{st})h_i^o + (1 - X_R)h_{ad}(Z) \tag{12}$$

The mass fractions of the chemical species are independent of the radiative heat loss fraction [39]. Inserting Eq. (10) into Eq. (12) yields

$$h(Z, \chi_{st}, X_R) = X_R \sum_i Y_i(Z, \chi_{st})h_i^o + (1 - X_R) \cdot (h_{ox}(1 - Z) + h_{fu}Z) \tag{13}$$

The Favre-averaged enthalpy may then be computed as

$$\tilde{h} = \int_0^1 h(Z, \chi_{st}, X_R)\tilde{P}(Z)\, dZ = X_R \sum_i \tilde{Y}_i h_i^o + (1 - X_R)(h_{ox}(1 - \tilde{Z}) + h_{fu}\tilde{Z}) \tag{14}$$

where Eq. (7) was used, and X_R was assumed to be independent of Z. This equation is used to compute X_R from $\tilde{Z}$, $\tilde{h}$, and $\tilde{Y}_i$, with $\tilde{h}$ given from the solution of its transport equation, and $\tilde{Y}_i$ given from Eq. (7) for the local value of $\tilde{\chi}_{st}$.

An implicit equation for the temperature as a function of Z, $\tilde{\chi}_{st}$, and X_R is obtained from Eqs. (9) and (13):

$$T = T^o + \frac{(1 - X_R)\left[h_{ox}(1 - Z) + h_{fu}Z - \sum_i Y_i h_i^o\right]}{\bar{c}_p} \tag{15}$$

where

$$\bar{c}_p = \frac{\sum_i Y_i \int_{T^o}^{T} c_{p,i}\, dT}{T - T^o} \tag{16}$$

Finally, the mean temperature is calculated from

$$\tilde{T} = \int_0^1 T(Z, \tilde{\chi}_{st}, X_R)\tilde{P}(Z)\, dZ \tag{17}$$

or

$$\bar{T} = \bar{\rho}\int_0^1 \frac{T(Z, \tilde{\chi}_{st}, X_R)}{\rho(Z, \tilde{\chi}_{st}, X_R)}\tilde{P}(Z)\, dZ \tag{18}$$

where the overbar denotes the Reynolds average. The mean density is computed from the ideal gas law:

$$\bar{\rho} = \left[\int_0^1 \frac{\tilde{P}(Z)}{\rho(Z, \tilde{\chi}_{st}, X_R)}\, dZ\right]^{-1} = \left[\int_0^1 \frac{R_o T(Z, \tilde{\chi}_{st}, X_R)}{p} \sum_i (Y_i(Z, \tilde{\chi}_{st})/W_i)\tilde{P}(Z)\, dZ\right]^{-1} \tag{19}$$

where R_o is the universal gas constant and W_i is the molar weight of species i.

2.3. Gas radiation properties model

The radiative properties of the gas mixture are computed using the SLW model. This model is summarized below for the sake of completeness. In a mixture with two participating gases, namely CO_2 and H_2O, the total emissivity, ε_g, may be written as

$$\varepsilon_g = \sum_{k=0}^{N_g} \sum_{j=0}^{N_g} a_{jk}[1 - \exp(-\kappa_{jk}L)] \tag{20}$$

where indices j and k identify the jth gray gas component for H_2O and the kth gray gas component for CO_2, N_g is the number of gray gases and L is the path length. The values $j = 0$ and $k = 0$ account for the spectral windows where H_2O and CO_2 are transparent to radiation, respectively. It is assumed here that the contribution from other radiating species, such as CO and CH_4, is negligible. The contribution from CO in the combustion gases is negligible, as long as its concentration does not exceed relatively high values of the order of 5% [58], while the contribution from CH_4 is even lower than that of CO.

The weight a_{jk} in Eq. (20) is defined as the fraction of blackbody energy in the spectrum where the effective absorption cross-section of H_2O is C_{wj} and where the effective absorption cross-section of CO_2 is $C_{c,k}$. The spectral regions where the effective absorption cross-section is $C_{s,j}$ are those where the absorption cross-section is between $\tilde{C}_{s,j}$ and $\tilde{C}_{s,j+1}$, with subscript s standing for the chemical species (w or c). The supplemental absorption cross-sections, denoted with a tilde, are used to calculate the weights a_{jk}, but they do not appear directly in the corresponding gray gas absorption coefficients κ_{jk}. The absorption cross-section domain is divided into N_g intervals, equally spaced in a logarithmic scale, provided that N_g is large enough, typically 10 or 20. The limits of each interval define the values of the supplemental absorption cross-sections $\tilde{C}_{s,j}$. The absorption cross-sections $C_{s,j}$ are computed as follows

$$C_{s,j} = \exp\,[(\ln \tilde{C}_{s,j} + \ln \tilde{C}_{s,j+1})/2] \tag{21}$$

The weights a_{jk}, which add up to unity, are calculated according to the double integration approach [59], yielding

$$a_{jk} = [F_w(\tilde{C}_{w,j+1}) - F_w(\tilde{C}_{w,j})][F_c(\tilde{C}_{c,k+1}) - F_c(\tilde{C}_{c,k})] \tag{22}$$

The absorption-line blackbody distribution function, F_s, is defined as the fraction of the blackbody energy in the portions of the spectrum where the high-resolution spectral absorption cross-section of the gas, $C_{s,\eta}$, is less than a prescribed value C_s:

$$F_s(C_s, T_b, T_g, P_T, X_s) = \frac{1}{\sigma T_b^4} \sum_i \int_{\Delta\eta_i(C_s,T_g,P_T,X_s)} E_{b\eta}(\eta, T_b)\, d\eta \tag{23}$$

where σ is the Stefan-Boltzmann constant and $E_{b\eta}$ is the spectral emissive power of a blackbody evaluated at wave number η and blackbody (source) temperature T_b. The subscript i refers to the ith spectral segment where $C_{s,\eta} < C_s$, which depends on C_s, gas temperature, T_g, total pressure, P_T, and molar fraction of species s, X_s. The correlations for F_w and F_c given in [60] and [61], respectively, were employed in all the calculations reported below.

The absorption coefficients κ_{jk} in Eq. (20) are calculated as

$$\kappa_{jk} = N_w C_{w,j} + N_c C_{c,k} \tag{24}$$

where N_w and N_c are the molar densities of H_2O and CO_2, respectively.

In the general case of a nonisothermal and/or nonhomogeneous medium, the absorption cross-sections defined by Eq. (21) are associated with a reference state defined by a temperature, T_{ref}, a total pressure, $P_{T,ref}$, and molar fractions $X_{s,ref}$, and are denoted by $C_{s,ref}$. That reference state is determined as the spatial average of the temperature, total pressure, and chemical composition fields. The absorption-line blackbody distribution functions in Eq. (22) are calculated for $T_g = T_{ref}$, $P_T = P_{T,ref}$, $X_s = X_{s,ref}$, and $T_b = T_{loc}$ or $T_b = T_{wall}$ depending on the source of radiation being the gas or the wall. Here, T_{loc} is the local gas temperature and T_{wall} is the wall temperature. The local molar densities and the absorption cross-sections in Eq. (24) are both evaluated from the local properties, identified with subscript *loc*, i.e., $T_g = T_{loc}$, $P_T = P_{T,loc}$ and $X_s = X_{s,loc}$. The local values of the absorption cross-section, C_s, in that equation are calculated from the following implicit equation [62]:

$$F_s\lfloor C_s, T_b = T_{ref}, T_g = T_{loc}, X_s = X_{s,loc}, P_T = P_{T,loc}\rfloor = F_s[C_{s,ref}, T_b = T_{ref}, T_g = T_{ref}, X_s = X_{s,ref}, P_T = P_{T,ref}] \tag{25}$$

where the reference absorption cross-sections, $C_{s,ref}$, are determined from Eq. (21), as stated above. Equation (25) is solved at each spatial location using an iterative method.

The total number of gases, N_g, ranges between 10 and 20. However, it is possible to achieve good accuracy with only $N_g = 3$ by means of an optimization procedure based on the minimization of the

squared relative error in emissivity over the range of path lengths typical of the flame under investigation, and for the temperature and species concentrations at the reference state [25]. In such a case, Eq. (21) is not used, and the absorption cross-sections as well as the supplemental absorption cross sections at the reference state are determined from the optimization procedure. Eq. (25) is still used to calculate the absorption cross-sections at the local conditions. This strategy was used in the present work.

2.4. Radiation model

The code for radiative transfer calculations is based on the DOM. The radiative transfer equation for the jth gray gas component of H_2O and the kth gray gas component of CO_2 may be written as follows [23]:

$$\frac{dI_{jk}}{ds} = -\kappa_{jk} I_{jk} + a_{jk}\kappa_{jk} I_b \tag{26}$$

where I_{jk} is the radiation intensity for those gray gas components, s is the direction of propagation of radiation, and I_b is the blackbody radiation intensity. Scattering has been neglected, since it is not present in the case of a gaseous non-luminous flame. This equation is time-averaged to account for the TRI, yielding

$$\frac{d\bar{I}_{jk}}{ds} = -\overline{\kappa_{jk} I_{jk}} + \overline{a_{jk}\kappa_{jk} I_b} \tag{27}$$

The difficulty with this equation is the correlation between the radiation intensity and the absorption coefficient in the first term on the right side. Following Song and Viskanta [38], it will be assumed that the individual eddies are homogeneous, optically thin, and statistically independent. The accuracy of this method was recently investigated by means of radiative transfer calculations along lines of sight of the same flame considered here. The results are reported in [63] and show that the predictions obtained using the DOM together with the SLW model and the optically thin eddy approximation of Song and Viskanta [38] for the TRI are within 4% of the results obtained using the stochastic method by Chan and Pan [35], which were taken as benchmark. This shows that the method of Song and Viskanta is reasonably accurate for the present flame.

According to this method, the correlation on the right of Eq. (27) may be approximated by

$$-\overline{\kappa_{jk} I_{jk}} \approx -\bar{\kappa}_{jk}\bar{I}_{jk} \tag{28}$$

and so Eq. (27) may be simplified as

$$\frac{d\bar{I}_{jk}}{ds} = -\bar{\kappa}_{jk}\bar{I}_{jk} + \overline{a_{jk}\kappa_{jk} I_b} \tag{29}$$

The boundary condition for a gray diffuse surface may be written as

$$I_{w,jk} = \varepsilon_w a_{jk} I_{bw} + \frac{(1-\varepsilon_w)}{\pi} \int_{\mathbf{n}\cdot\mathbf{s}'<0} |\mathbf{n}\cdot\mathbf{s}'| I_{jk}(\mathbf{s}')\, d\Omega' \tag{30}$$

where ε_w is the surface emissivity, $\mathbf{n}$ is the unit vector normal to the surface, and $\mathbf{s}'$ is the direction of propagation of the incident radiation associated with the solid angle $d\Omega'$. In the present case $\varepsilon_w = 1$, because the boundary of the computational domain is treated as a blackbody at room temperature. The time-averaged form of the boundary condition is written as

$$\bar{I}_{w,jk} = \varepsilon_w a_{jk} I_{bw} + \frac{(1-\varepsilon_w)}{\pi} \int_{\mathbf{n}\cdot\mathbf{s}'<0} |\mathbf{n}\cdot\mathbf{s}'| \bar{I}_{jk}(\mathbf{s}')\, d\Omega' \tag{31}$$

Applying the DOM, the time-averaged equation for the jth component of H_2O, the kth component of CO_2, and the mth direction can be written in the form:

$$\frac{d\overline{I_{jk}^m}}{ds} = -\bar{\kappa}_{jk}\overline{I_{jk}^m} + \overline{a_{jk}\kappa_{jk} I_b} \tag{32}$$

The total radiation intensity for direction m is given by

$$I^m = \sum_{k=0}^{N_g} \sum_{j=0}^{N_g} I_{jk}^m \tag{33}$$

The discretization of Eq. (32) follows standard practices, as described in detail in [64,65]. That equation may be re-written in cylindrical coordinates as

$$\zeta^m \frac{\partial \overline{I_{jk}^m}}{\partial x} + \frac{\mu^m}{r}\frac{\partial (r\overline{I_{jk}^m})}{\partial r} - \frac{1}{r}\frac{\partial}{\partial \psi}(\eta^m \overline{I_{jk}^m}) = -\bar{\kappa}_{jk}\overline{I_{jk}^m} + \overline{a_{jk}\kappa_{jk} I_b} \tag{34}$$

where ζ^m, μ^m, and η^m are the direction cosines of the axial, radial and tangential directions, respectively, given by

$$\begin{aligned} \mu^m &= \sin\theta_m \cos\psi_m, \\ \eta^m &= \sin\theta_m \sin\psi_m, \\ \zeta^m &= \cos\theta_m \end{aligned} \tag{35}$$

Here, ψ is the azimuthal direction angle, measured from the local radial direction. The 3rd term on the left of Eq. (34) is discretized as follows, for fixed ζ^m:

$$\frac{\partial}{\partial \psi}(\eta^m \overline{I_{jk}^m}) \approx (\alpha_{m+1/2}\overline{I_{jk}^{m+1/2}} - \alpha_{m-1/2}\overline{I_{jk}^{m-1/2}})/w_m \tag{36}$$

The directions $m \pm 1/2$ define the edges of angle $\Delta\psi$ associated with direction m, and w_m is the quadrature weight for that direction. The geometrical coefficients α satisfy the following relation, drawn on the basis of isotropic radiation

$$\alpha_{m+1/2} - \alpha_{m-1/2} = w_m \mu^m \tag{37}$$

The coefficient $\alpha_{1/2}$ is equal to zero [64]. The coefficients $\alpha_{m+1/2}$ for the other directions are determined recursively from Eq. (37). The integration of Eq. (34) over a control volume yields

$$\begin{aligned}|\zeta^m| A_x(\overline{I_{jk,x,out}^m} - \overline{I_{jk,x,in}^m}) + |\mu^m|(A_{r,out}\overline{I_{jk,r,out}^m} \\ - A_{r,in}\overline{I_{jk,r,in}^m}) - |A_{r,out} - A_{r,in}| \\ \frac{\alpha_{m+1/2}\overline{I_{jk,P}^{m+1/2}} - \alpha_{m-1/2}\overline{I_{jk,P}^{m-1/2}}}{w_m} \\ = (-\bar{\kappa}_{jk}\overline{I_{jk,P}^m} + \overline{a_{jk}\kappa_{jk}I_{b,P}})V\end{aligned} \tag{38}$$

where A are the areas of the cell faces and V is the volume. The indices *in* (*out*) denote a cell face where radiation flows into (out from) the control volume, and the subscripts r and x stand for the radial and axial directions, respectively. The subscript P identifies the control volume under consideration. The radiation intensities at the cell faces have been calculated according to the STEP discretization scheme:

$$\overline{I_{jk,x,out}^m} = \overline{I_{jk,r,out}^m} = \overline{I_{jk,P}^{m+1/2}} = \overline{I_{jk,P}^m} \tag{39}$$

Inserting Eqs. (39) into Eq. (38), an explicit relation for the radiation intensity at point P is obtained.

The solution algorithm requires the solution of a set of M ($1 \le m \le$ M) differential equations (Eq. (34)) for every j and k gray gas component of H_2O and CO_2, respectively. These equations are decoupled, because there is no scattering, and may be efficiently solved as described in [64,65].

The source term of the transport equation for enthalpy is given by

$$\overline{\nabla \cdot \mathbf{q}} = \sum_{k=0}^{N_g}\sum_{j=0}^{N_g}\left(4\pi\overline{a_{jk}\kappa_{jk}I_b} - \bar{\kappa}_{jk}\sum_{m=1}^{M} w_m \overline{I_{jk}^m}\right) \tag{40}$$

The above equations show that the mean value of the absorption coefficient κ_{jk}, as well as the mean value of the product $a_{jk}\kappa_{jk}I_b$, are required to account for the TRI. The absorption coefficient depends on the molar fractions of H_2O and CO_2, the weight a_{jk} is a function of the same molar fractions and temperature, and I_b is a function of the temperature. Furthermore, the molar fractions of H_2O and CO_2 and the temperature depend on the mixture fraction and scalar dissipation rate, and in addition the temperature depends on the radiative heat loss fraction. Therefore, the required mean values were computed by means of integration over the mixture fraction range, taking into account all the dependences referred above:

$$\bar{\kappa}_{jk} = \bar{\rho}\int_0^1 \frac{\kappa_{jk}(Z, \tilde{\chi}_{st})}{\rho(Z, \tilde{\chi}_{st}, X_R)}\tilde{P}(Z)\, dZ \tag{41}$$

$$\overline{a_{jk}\kappa_{jk}I_b} = \bar{\rho}\int_0^1 \frac{a_{jk}(Z, \tilde{\chi}_{st}, X_R)\kappa_{jk}(Z, \tilde{\chi}_{st})I_b(Z, \tilde{\chi}_{st}, X_R)}{\rho(Z, \tilde{\chi}_{st}, X_R)}\tilde{P}(Z)\, dZ \tag{42}$$

3. Computational details

The computational domain extends from $x/d = 0$ to $x/d = 150$, and from $r/d = 0$ to $r/d = 50$, where d is the diameter of the fuel nozzle. A non-uniform grid with 200×90 grid nodes was used, with the grid nodes concentrated close to the centreline, in such a way that 16 grid nodes in the radial direction are placed inside the fuel jet, and 22 grid nodes are inside the pilot fuel flame. The radiative transfer calculations were performed using the same spatial grid, and the T_7 quadrature [66]. The SLW model requires the definition of a reference state. To define this reference state, only the subdomain where the local mixture fraction exceeds 5% of the stoichiometric mixture fraction was considered. The subdomain where the local mixture fraction is below that value corresponds to points which are sufficiently far from the flame region, so that they should not influence a reference state that is representative of average conditions in the flame region. It was checked that this threshold of 5% has no influence on the predictions. The boundary conditions at the inlet sections are prescribed according to the recommendations reported in [45].

The flamelet profiles for the species concentrations were generated using a computer code and a detailed chemical mechanism developed at ITM-RWTH, as described in [52]. A flamelet library was generated for values of the scalar dissipation rate ranging from a low value close to chemical equilibrium to a large value close to extinction ($0.1\ s^{-1}$ and $200\ s^{-1}$, respectively, for the present flame). The mean values of species mass fractions are computed

a priori, that is, before executing the BIGMIX code, for a discrete representative set of values of mixture fraction, mixture fraction variance, and scalar dissipation rate, and the results are stored in three-dimensional tables. Similarly, the mean values of temperature and density are calculated *a priori* for the same discrete set of parameters plus one additional parameter, the fraction of radiative heat loss. They are based on the flamelet profiles for species and temperature in adiabatic conditions, and in Eq. (15) for non-adiabatic conditions. The results are stored in four-dimensional tables. The mean values given by Eqs. (41) and (42) are also calculated *a priori*, and stored in four-dimensional tables. During the flame simulation, the mean values of these quantities are obtained from interpolation of the stored data, rather than by explicit evaluation of the integrals.

The numerical accuracy was checked by comparing the predicted results calculated using the grid mentioned above with those obtained using a coarser grid with 80 grid nodes in the axial direction. It was found that the two sets of results were very close to each other, and therefore may be regarded as grid independent.

The calculations were performed using a workstation with an AMD Athlon Duron 750 MHz processor. The radiative transfer calculations are performed only after a reasonably converged solution has been achieved, and only every 20 iterations of the CFD code. Each CFD iteration requires 12.5 s of CPU time. The computational requirements for radiative transfer depend on the selected modeling approach. The CPU time for the optically thin approximation is negligible, while the DOM requires about 4.2 s per call to the radiation solver in the case of a gray medium, and 67 s in the case of a non-gray medium dealt with the SLW model. The ratio between these two values is 16, which corresponds to the number of times that the radiative transfer equation is solved to account for all the gray gas components in the SLW model ($N_g = 3$ in Eq. (21)). This does not include the time required to compute the radiative properties of the medium. The calculation of these properties requires less than 2 s for a gray medium if the TRI is neglected or accounted for only via $\bar{I}_b$, and 27 s if the TRI if fully accounted for. If the SLW model is used, then 21 s and 148 s are needed, depending on whether the TRI is fully taken into account or not. No efforts were made to optimize these times, for example, it is likely that a lower order quadrature can be employed in the DOM without significant influence on the accuracy.

4. Experimental configuration

The piloted methane/air jet flame investigated in this study was experimentally studied in [67], the so-called flame D, and the experimental data are available in [45]. The piloted burner has a main jet diameter of 7.2 mm and a pilot with an inner diameter of 7.7 mm and an outer diameter of 18.2 mm. The fuel jet mole composition is 25% CH_4 and 75% air at 294 K. The annular pilot burns a mixture of C_2H_2, H_2, air, CO, and N_2, with the same enthalpy and equilibrium composition as methane/air at 0.77 equivalence ratio ($Z = 0.27$), and at 1880 K. The fuel jet Reynolds number is 22400. The mean velocities of the fuel and pilot jets are 49.6 and 11.4 m/s, respectively. In addition, there is a coflow of air with a velocity of 0.9 m/s. At these conditions, the flame burns as a diffusion flame, and no evidence of premixed reaction in the fuel-rich methane/air mixture was found.

5. Results and discussion

The calculations were carried out for six different situations:

1. Adiabatic flame.
2. Optically thin flame. In this case the radiative transfer equation is not solved, and the source term of the enthalpy equation is calculated from

$$\overline{\nabla \cdot \mathbf{q}} = 4\kappa\sigma(\overline{T^4} - T_\infty^4) \tag{43}$$

where κ is the absorption coefficient and T_∞ is the background temperature. The absorption coefficient is calculated as recommended in [45], i.e., using the curve fits for the Planck mean absorption coefficients of H_2O, CO_2, CO, and CH_4. The TRI is partially taken into account by using $\overline{T^4}$ rather than $\bar{T}^4$ in the evaluation of the source term. However, the TRI is not fully accounted for, because the correlation $\overline{kT^4}$ in the emission term is ignored and approximated as $\kappa\overline{T^4}$, and κ is calculated using the local mean temperatures and mean species concentrations.
3. The radiative transfer equation is solved using the DOM, and the Planck-mean absorption coefficient, hereafter denoted by κ_P, is calculated as in Case 2. The TRI is only accounted for in the evaluation of $\bar{I}_b$, i.e., $\overline{T^4}$ rather than $\bar{T}^4$ is used to calculate $\bar{I}_b$. However, the turbulent fluctuations are ignored in the calculation of the mean absorption coefficient, and the cor-

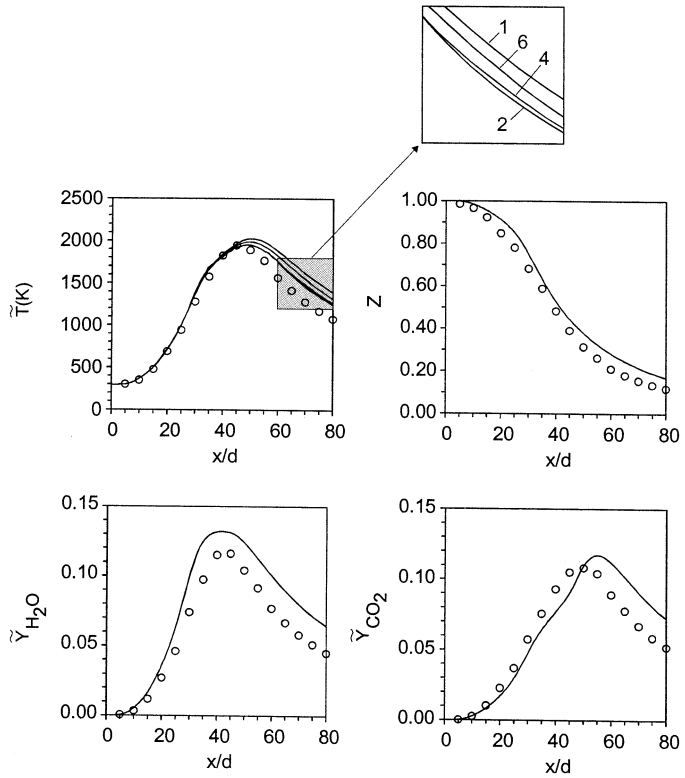

Fig. 1. Predicted and measured axial profiles of temperature, mixture fraction, H_2O and CO_2 mass fractions.

relation between the absorption coefficient and the blackbody emissive power is neglected. This is the most common approach in flame radiation calculations whenever the radiative transfer equation is solved.

4. The radiative transfer equation is solved using the DOM, κ_P is calculated as in Case 2, and the TRI is fully accounting for, i.e., $\bar{\kappa}$ and $\overline{\kappa I_b}$ are calculated from equations similar to Eqs. (41) and (42).
5. The radiative transfer equation is solved using the DOM, the gas radiative properties are calculated using the SLW model, and the TRI is only taken into account in the evaluation of $\bar{I}_b$.
6. The radiative transfer equation is solved using the DOM, the gas radiative properties are calculated using the SLW model, and the TRI is fully accounted for as described before.

The predicted temperature, mixture fraction, H_2O, and CO_2 mass fraction profiles along the centreline are plotted in Fig. 1 along with the experimental data. The temperature is accurately predicted up to the measured stoichiometric length, $L_{\text{stoich}} = 47d$. Up to this distance, radiation is of marginal importance, since in this part of the flame the temperature is determined by the rate of turbulent combustion. The maximum predicted temperature occurs slightly downstream of the maximum measured temperature. Further downstream, the temperature is overpredicted, regardless of the radiation model. This is consistent with the overprediction of mixture fraction and combustion products (H_2O and CO_2) downstream of L_{stoich}. Radiation plays a more important role in this region, as expected [68].

The radial temperature profiles at stations $x/d = 30$, 45, 60, and 75, which are given in Figs. 2 to 5, respectively, suggest that the spreading rate of the fuel jet is overestimated, even though the $C_{\varepsilon 1}$ constant of the turbulence model has been decreased to improve this. In the vicinity of the centreline the mass fractions of H_2O and CO_2, plotted in the same figures, are also overpredicted, except the CO_2 mass fraction at $x/d = 30$ and 45. The overprediction of temperature, H_2O and CO_2 mass fractions contribute to overestimate the radiative heat loss.

The variations in the temperature predictions using different radiation models are of the same order of magnitude as the systematic uncertainty of the temperature measurements (3%, as reported in [67]). Moreover, the difference between the temperatures calculated with radiation and those computed for adiabatic conditions do not exceed 150 K, no matter

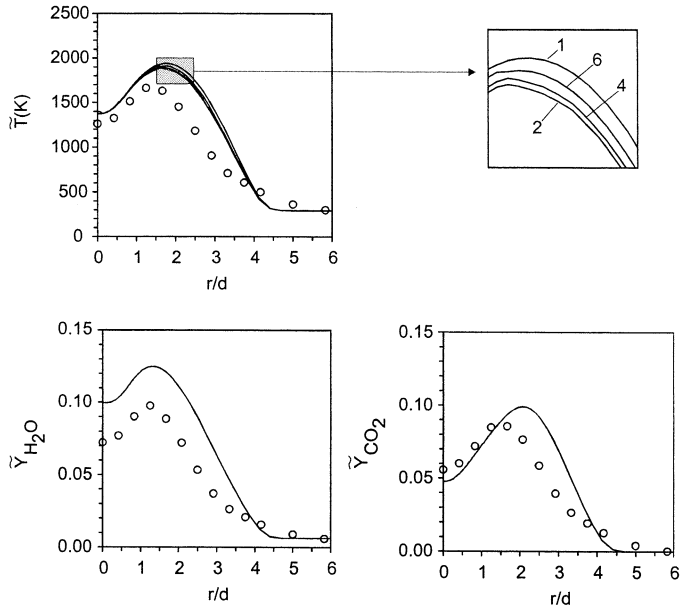

Fig. 2. Predicted and measured radial profiles of temperature, H_2O and CO_2 mass fractions at $x/d = 30$.

the radiation model employed, and it is somewhat difficult to distinguish the different curves in Figs. 1 to 5. Therefore, enlarged views of the temperature profiles are provided in those figures to highlight the difference between the modeling approaches. The temperature profiles for Cases 3 and 5 are not shown because they are almost coincident with the profiles for Cases 4 and 6, respectively. The mixture fraction and major species mass fraction profiles are almost coincident for all cases, and therefore they have only been plotted for Case 6. However, it is worth noting that although the radiation loss from the flame is relatively small, its influence on the temperature distribution may have an important impact on the NO emission, as discussed in [67].

It is clear from the temperature profiles that if κ_P

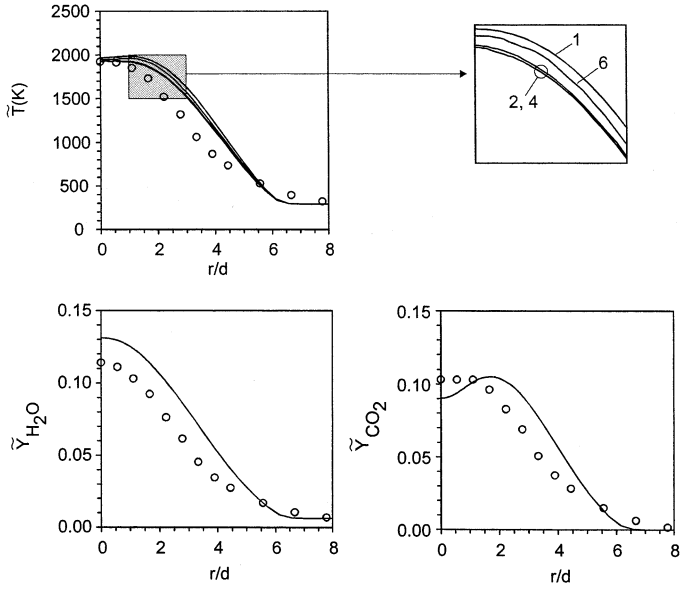

Fig. 3. Predicted and measured radial profiles of temperature, H_2O and CO_2 mass fractions at $x/d = 45$.

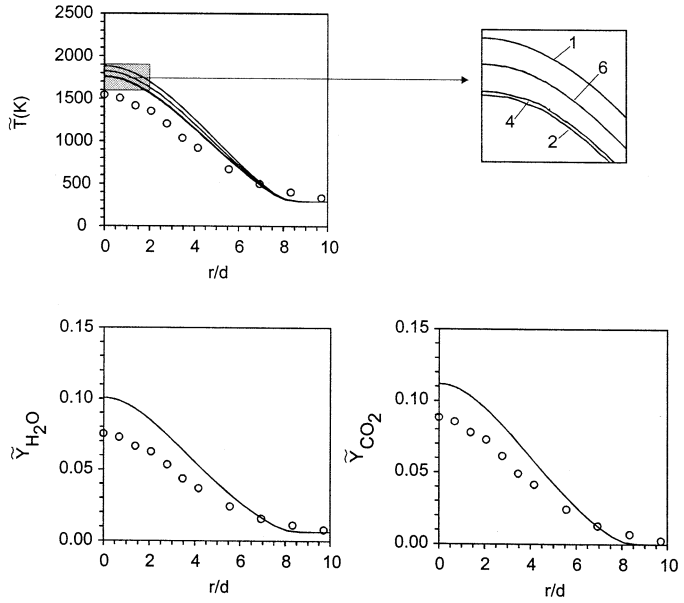

Fig. 4. Predicted and measured radial profiles of temperature, H_2O and CO_2 mass fractions at $x/d = 60$.

is employed, then the DOM (Cases 3 and 4), which accounts for both gas emission and absorption, and the optically thin approximation (Case 2), which only accounts for emission, give relatively close results. However, the radiative heat loss for the optically thin approximation is larger, and the temperatures lower, than for the DOM, because absorption is neglected in the former case. If the medium is modeled as non-gray using the SLW approach (Cases 5 and 6), then the predicted temperatures are lower than those in adiabatic conditions (Case 1), but higher than the temperatures calculated using the DOM/gray gas assumption (Cases 3 and 4) or the optically thin approximation (Case 1).

Figs. 1 to 5 show that, for all the radiation models, the mean temperature and the mean mass fractions of H_2O and CO_2 are overpredicted compared with the experiments over a large part of the flame. Basically,

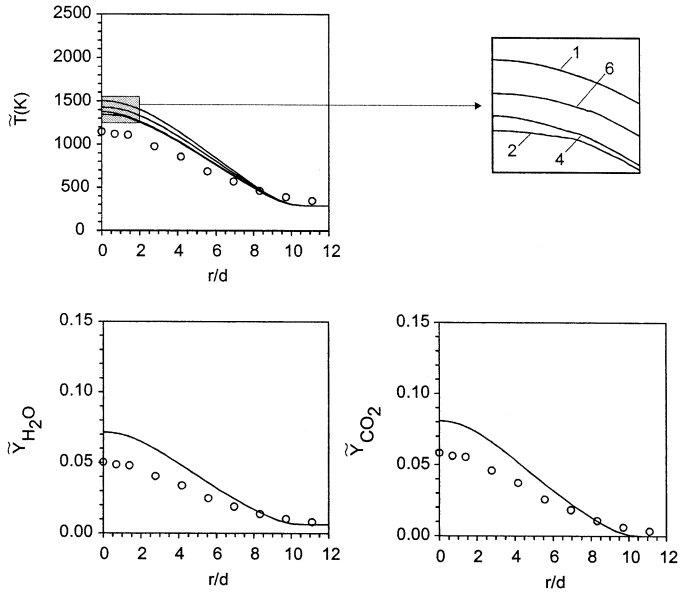

Fig. 5. Predicted and measured radial profiles of temperature, H_2O and CO_2 mass fractions at $x/d = 75$.

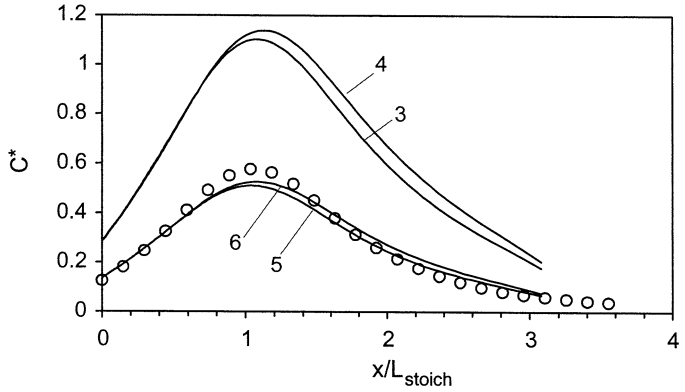

Fig. 6. Predicted and measured non-dimensional radiant power along the axial direction.

this has nothing to do with the choice of the radiation model, but shows a limitation of the other models, namely the turbulence and combustion models. Such discrepancies are common to all the predictions that have been reported for this flame, as described in the Proceedings of the recent Workshops on 'Measurement and Computation of Turbulent Nonpremixed Flames' available in [45]. Overall, our predictions are not far from the others. On the other hand, it was found that the radiant fraction strongly depends on the radiation model, as revealed in Fig. 6.

Fig. 6 shows the measured and predicted non-dimensional radiant power, C^*, along the axial direction, as defined in [46,69]:

$$C^* = \frac{4\pi R^2 q_R}{S_{rad,\exp}} \tag{44}$$

where q_R is the radiative heat flux, which is a function of the axial position, and R is the radius of the computational domain. C^* is non-dimensionalized by the measured total radiant power, $S_{rad,exp}$. The heat fluxes on the boundary cannot be computed using the optically thin approximation, and therefore, C^* is not given for Case 2. Fig. 6 shows that if the spectral nature of gaseous radiation is taken into account using the SLW model (Cases 5 and 6), the radiation loss is significantly lower than treating the medium as gray using κ_P (Cases 3 and 4), and a very satisfactory agreement with the experimental data is found. The TRI enhances the radiation loss, but it plays a secondary role in the present flame. However, the good agreement found in Cases 5 and 6 may be fortuitous, because the temperature and the H_2O and CO_2 mass fractions are generally overestimated, and therefore C^* should also be overestimated.

To further investigate this issue, we have performed additional calculations of radiative transfer based upon the measured temperature, H_2O and CO_2 mass fraction profiles. These calculations are decoupled from CFD. Therefore, errors arising from turbulence and combustion models do not influence these radiative calculations, except in the calculation of mean values not directly available from the experimental data, such as $\bar{I}_b$ and those in Eqs. (41) and (42). The calculation of these mean values assumes a clipped Gaussian pdf shape, defined from the measured mean and variance of mixture fraction. The relationships between instantaneous values of temperature/species and mixture fraction are also taken from experimental data. However, the experimental data is limited to the centreline profile up to $x/d = 80$ and to a few radial profiles up to $x/d = 75$. Therefore, the experimental data has been interpolated for $x/d \leq 75$, and extrapolated further downstream. This extrapolation is subject to uncertainties, which certainly influence the predictions to some extent. The results obtained are plotted in Fig. 7. It shows that the values of C^* are consistently lower than those in Fig. 6, as expected. However, C^* is again strongly overpredicted for Cases 2 and 3, while it is underpredicted for Cases 5 and 6.

The predicted total radiation heat loss for all the different methods is given in Table 1 along with the measured value. This corresponds to the integral of $\overline{\nabla \cdot \mathbf{q}}$ over the computational domain. The ratio of this value to the power released in combustion is the total fraction of radiative loss, ϕ_R, which is also given in Table 1. The optically thin approach overpredicts the radiation loss by a factor of 2.6 and 1.9, for coupled CFD/radiation and uncoupled radiative calculations, respectively, i.e., it estimates a radiative heat loss fraction close to that obtained in the calculations reported in [46], using also the optically thin approximation. As mentioned before, in that work radiant fractions of 10.5% and 12.5% were computed using the PDF and the CMC combustion models, respectively. In the former case the calculations were performed up to a downstream location of $x/d = 90$,

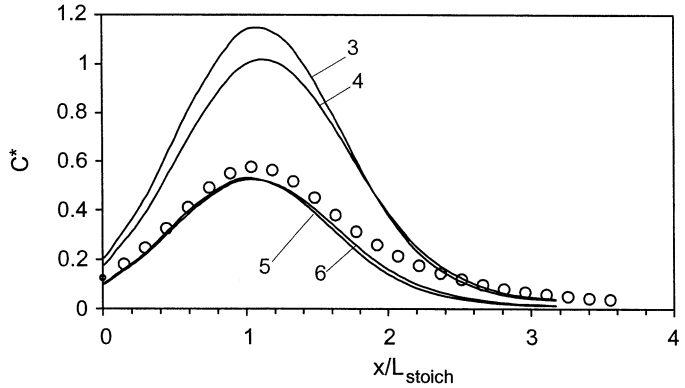

Fig. 7. Predicted and measured non-dimensional radiant power along the axial direction. The predicted values are based on temperature and species concentration fields interpolated and extrapolated from the experimental data.

and in the second case up to $x/d = 100$. However, the region downstream of $x/d = 100$ ($x/L_{stoich} = 2.13$) still contributes to the radiation loss, although that contribution is relatively small, as shown in Figs. 6 and 7. Therefore, the total fraction of radiation loss for the whole flame would exceed 12.5% according to those results. The calculations reported in [47], using again the optically thin approximation, predict a value of 2.85% for the radiant fraction up to $x/d = 60$. Therefore, they approach the measured value of $\phi_R = 5.1\%$ for the whole flame, because only 50–60% of the total radiation loss occurs up to that axial station. Nevertheless, they are in contradiction with our calculations and with those described in [46], which both predict a much higher radiative loss when the optically thin approximation is employed.

More accurate results are expected if radiative transfer is calculated using the DOM, which is based on the numerical solution of the RTE. However, if κ_P is used, then ϕ_R is still too large compared with the experimental data. In fact, Table 1 shows that $\phi_R = 11.4\%$ in Case 3, and $\phi_R = 12.1\%$ in Case 4, for coupled CFD/radiative calculations. The corresponding values for uncoupled calculations are lower, but still too high if compared with the experimental data.

The most accurate predictions are obtained using the SLW model, which accounts for the spectral nature of gaseous radiation. In the case of coupled CFD/radiative calculations, ϕ_R is slightly underestimated if the TRI is only accounted for via $\bar{I}_b$ (Case 5), and marginally overpredicted if the TRI is fully taken into account (Case 6). However, this good agreement relies upon computed temperature and species concentration fields that tend to overestimate the experimental data, as discussed above. If uncoupled radiative calculations are carried out, then ϕ_R is underestimated by about 25% for both Cases 5 and 6.

From the results obtained, it can be concluded that the DOM along with κ_P yields only a marginal improvement of the radiative heat loss over the optically thin approximation. In the former case, and accounting for the TRI only via $\bar{I}_b$ (Case 3), the radiative heat source is given by

$$\overline{\nabla \cdot \mathbf{q}} = \kappa(4\pi\bar{I}_b - G) \tag{45}$$

Table 1
Predicted and measured radiative heat loss and fraction of radiative heat loss

Test Case	Coupled CFD/Radiation calculations		Radiative calculations based on experimental data	
	Radiative heat loss (kW)	Fraction of radiative heat loss (%)	Radiative heat loss (kW)	Fraction of radiative heat loss (%)
Experimental	0.887	5.1	0.887	5.1
2	2.349	13.6	1.647	9.5
3	1.968	11.4	1.503	8.7
4	2.090	12.1	1.378	8.0
5	0.868	5.0	0.656	3.8
6	0.911	5.3	0.672	3.9

Table 2
Predicted total radiation intensity (W/m^2st) at the end of the radial line of sight at $x/d = 45$

	Emission and absorption	Emission only
RADCAL (narrow band model)	4363	6021
Analytical integration of the radiative transfer equation using κ_P	6233	6533

where G is the incident radiation, while in the second case it is given by Eq. (43). Hence, emission is calculated in the same way by the two models, and this implies that the difference between them is due to absorption. A comparison between the results computed for the two terms into parenthesis in Eq. (45) has shown that the first term is at least one order of magnitude larger than the incident radiation, except in the coldest regions of the flame. This explains why the DOM results using κ_P (Cases 3 and 4) yield only a small improvement of the predicted fraction of radiative heat loss compared with the optically thin results.

The RADCAL code [70], which is based on the Goody narrow band model [71], was used in [46] to calculate the spectral radiation intensity along the radial cross section at $x/d = 45$. The measured species and temperature profiles were used as input data. According to these calculations, which have been confirmed by us, if only emission is accounted for, then the total radiated power is 39% higher than that of the emission-absorption computation. The values obtained are given in Table 2, along with those obtained from the analytical solution of the radiative transfer equation using κ_P. It can be seen that the emission-only calculations performed using κ_P differ by less than 10% from the narrow band results. However, the emission-absorption results differ by more than 40%. The gray gas calculations are marginally affected by absorption, contrary to the spectral calculations, and predict a significantly higher radiation intensity. This is entirely consistent with a radiative heat loss significantly higher when κ_P is used (Cases 3 and 4) than in the SLW computations (Cases 5 and 6). The reason for this behavior lies in the error resultant from using κ_P to calculate absorption, as discussed below.

Accounting for the TRI only via $\bar{I}_b$, the exact radiative source term is given by

$$\overline{\nabla \cdot \mathbf{q}} = \int_0^\infty \kappa_\eta \left(4\pi \bar{I}_b - \int_{4\pi} I_\eta \, d\Omega \right) d\eta$$

$$= 4\pi \kappa_P \bar{I}_b - \int_0^\infty \kappa_\eta \int_{4\pi} I_\eta \, d\Omega \, d\eta \qquad (46)$$

The emission term is correctly represented using κ_P, but not the absorption one [70]. The use of κ_P in the absorption term involves the following approximation

$$\int_0^\infty \kappa_\eta \int_{4\pi} I_\eta \, d\Omega \, d\eta \approx \kappa_P \int_0^\infty \int_{4\pi} I_\eta \, d\Omega \, d\eta$$

$$= \kappa_P G \qquad (47)$$

However, this may be a rather crude approximation in the present case. In fact, we have computed both terms of this equation using the SLW method, and it was found that the first term is about one order of magnitude larger than the second one over a large part of the flame. Therefore, it can be concluded that radiative calculations using κ_P obtained from RADCAL are expected to overestimate the radiative heat loss, in agreement with what we, as well as other researchers [46], have found.

The SLW model provides more accurate results, but the uncoupled radiative calculations based upon the experimental data underpredict the fraction of radiative heat loss by about 25%. There are several reasons that may explain this discrepancy. Among these are the interpolation of experimental data, and specially the extrapolation downstream of $x/d = 75$, the modeling assumptions inherent to the SLW model, the experimental errors of the spectroscopic data base from which the absorption-line blackbody distribution function is obtained, and the role of CO and CH_4, which has been neglected. Another source of error that may be important is the experimental error in temperature. In fact, an error of 3% in the temperature yields an error of about 12% in I_b.

Additional coupled CFD/radiative calculations were performed using $\bar{T}^4$ rather than $\bar{I}_b = \overline{T^4}$ in the calculation of the emission term of the radiative transfer equation, i.e., fully ignoring the TRI. The predicted radiative heat loss was 1.601 kW for the DOM/gray gas calculations, and 0.709 kW for the DOM/SLW calculations. This means that the predicted radiation heat loss increases by about 30% for the present flame when the TRI is fully simulated, for both gray and non-gray simulations.

The radiation loss from the present flame is relatively low. Therefore, the increase in accuracy resultant from the full simulation of the TRI may not

justify the significant increase in CPU time. However, in a flame with high radiation loss this simulation is certainly worthwhile.

6. Conclusions

A piloted turbulent jet methane/air diffusion flame was numerically simulated using the Reynolds stress closure for turbulence modeling and the steady laminar flamelet combustion model. Several different methods to compute the radiative transfer were compared. The optically thin approximation and the discrete ordinates method were used. The medium was treated either as gray, using the Planck mean absorption coefficient, or as non-gray, using the SLW model. The influence of the turbulence/radiation interaction on the radiative heat loss was investigated. From the analysis carried out it can be concluded that the spectral nature of gaseous radiation must be taken into account to obtain an accurate prediction of the radiative heat loss. If the medium is treated as gray, the fraction of radiative heat loss is overestimated by a factor of two or more. The calculations carried out using the DOM and the SLW model yield better results. Although the predicted radiative heat loss is in good agreement with the experimental data, the temperature and the absorbing species concentration fields were overestimated. Therefore, additional radiative calculations based on the experimental data were carried out. These confirm the trends observed in the coupled CFD/radiative calculations, but the total fraction of radiative heat loss is underpredicted by about 25% for the DOM/SLW model. The interaction between turbulence and radiation enhances the radiation loss by a factor of about 30% in the studied flame. If this interaction is only accounted for via the blackbody radiation intensity, i.e., if the fluctuations of the species are ignored, the results are similar to those computed accounting for the full interaction. Although the spectral effects of gaseous radiation and the interaction between turbulence and radiation have no major influence on the predicted temperature field for the present flame, owing to its low radiation loss, they will certainly become more relevant in highly radiating flames, particularly if gas radiation is dominant over particle radiation.

Acknowledgments

This work was financially supported by the European Commission in the framework of the TMR Network Contract No. ERBFMRX-CT98-0224 (RADIARE), and by the PRAXIS XXI Programme of the Portuguese Ministry of Science and Technology under contract PRAXIS/P/EME/12034/1998.

References

[1] J.H. Kent, D. Honnery, Combust. Sci. Tech. 54 (1987) 383.
[2] H.C. Hottel, E.S. Cohen, AIChE J. 4 (1958) 3.
[3] J.R. Howell, in: J.P. Hartnett, T.F. Irvine (Eds.), Advances in Heat Transfer, Vol. 5, Academic Press, New York, 1968, p. 1.
[4] Y. Bayazitoglu, J. Higenyi, AIAA J. 17 (1979) 424.
[5] F.C. Lockwood, N. Shah, Eighteenth Symposium (International) on Combustion, The Combustion Institute, Pittsburgh, 1981, p. 1405.
[6] S. Chandrasekar, Radiative Transfer, Dover Publications, New York, 1960.
[7] A. Mbiock, R. Weber, Radiation in Enclosures—Elliptic Boundary Value Problems, Springer-Verlag, Heidelberg, 1999.
[8] N. Lallemant, A. Sayre, R. Weber, Progress Energy Combust. Sci. 22 (1996) 543.
[9] S.-M. Jeng, M.-C. Lai, G.M. Faeth, Combust. Sci. Tech. 40 (1984) 41.
[10] A. Soufiani, E. Djavdan, Combust. Flame 97 (1994) 240.
[11] D.K. Edwards, in: T.F. Irvine, Jr., J.P. Hartnett (Eds.), Advances in Heat Transfer, Vol. 12, Academic Press, New York, 1976, p. 115.
[12] P. Docherty, M. Fairweather, Combust. Flame 71 (1988) 79.
[13] Y. Liu, B. Rogg, Combust. Sci. Technol. 118 (1996) 127.
[14] P.S. Cumber, M. Fairweather, H.S. Ledin, Int. J. Heat Mass Transfer 41 (1998) 1573.
[15] L. Zhang, A. Soufiani, J. Taine, Int. J. Heat Mass Transfer 31 (1988) 2261.
[16] T.K. Kim, J.A. Menart, H.S. Lee, J. Heat Transfer 113 (1991) 946.
[17] R.M. Goody, Y.L. Yung, Atmospheric Radiation—Theoretical Basis, Oxford University Press, New York, 1989.
[18] P. Rivière, D. Scutaru, T. Soufiani, J. Taine, Proceedings of the Tenth International Heat Transfer Conference, Vol. 2, Brighton, U.K., 1994, p. 129.
[19] K.C. Tang, M.Q. Brewster, J. Heat Transfer 116 (1994) 980.
[20] H.C. Hottel, A.F. Sarofim, Radiative Transfer, McGraw Hill, New York, 1967.
[21] L. Pierrot, A. Soufiani, J. Taine, J. Quant. Spectrosc. Rad. Transfer 62 (1999) 523.
[22] P.J. Coelho, J. Quant. Spectrosc. Rad. Transfer 74 (2002) 307.
[23] M.F. Modest, J. Heat Transfer 113 (1991) 650.
[24] N.W. Bressloff, J.B. Moss, P.A. Rubini, Twenty-Sixth Symposium (International) on Combustion, The Combustion Institute, Pittsburgh, 1996, p. 2379.
[25] M.K. Denison, B.W. Webb, J. Heat Transfer 115 (1993) 1004.

[26] L. Pierrot, Ph. Rivière, A. Soufiani, J. Taine, J. Quant. Spectrosc. Rad. Transfer 62 (1999) 609.
[27] M.F. Modest, H. Zhang, in Proceedings of the 2000 IMECE, Vol. HTD-366-1, ASME, Orlando, FL, 2000, p. 75.
[28] H. Zhang, M.F. Modest, in Proceedings of the Third International Symposium on Radiative Transfer, Antalya, Turkey, 2001.
[29] G.M. Faeth, S.-M. Jeng, J. Gore, in: C.K. Lau, Y. Jaluria, W.W. Yuen, K. Miyasaka (Eds.), Heat Transfer in Fire and Combustion Systems, ASME, New York, 1985, p. 137.
[30] M.E. Kounalakis, J.P. Gore, G.M. Faeth, Twenty-Second Symposium (International) on Combustion, The Combustion Institute, Pittsburgh, 1988, p. 1281.
[31] M.E. Kounalakis, J.P. Gore, G.M. Faeth, J. Heat Transfer 111 (1989) 1021.
[32] Y.R. Sivathanu, M.E. Kounalakis, G.M. Faeth, Twenty-Third Symposium (International) on Combustion, The Combustion Institute, Pittsburgh, 1990, p. 1543.
[33] M.E. Kounalakis, Y.R. Sivathanu, G.M. Faeth, J. Heat Transfer 113 (1991) 437.
[34] S.H. Chan, X.C. Pan, J. Zhang, Twenty-Fifth Symposium (International) on Combustion, The Combustion Institute, Pittsburgh, 1994, p. 1115.
[35] S.H. Chan, X.C. Pan, J. Heat Transfer 119 (1997) 509.
[36] R.J. Hall, A. Vranos, Int. J. Heat Mass Transfer 37 (1994) 2745.
[37] W. Krebs, R. Koch, B. Ganz, L. Eigenmann, S. Wittig, Twenty-Sixth Symposium (International) on Combustion, The Combustion Institute, Pittsburgh, 1996, p. 2763.
[38] T.H. Song, R. Viskanta, J. Thermophys. Heat Trans. 1 (1986) 56.
[39] J.P. Gore, U.-S. Ip, Y.R. Sivathanu, J. Heat Transfer 114 (1992) 487.
[40] B.R. Adams, P.J. Smith, Combust. Sci. Tech. 109 (1995) 121.
[41] J.W. Hartick, M. Tacke, G. Früchtel, E.P. Hassel, J. Janicka, Proceedings of The Combustion Institute, 26 (1996) 75.
[42] S. Mazumder, M.F. Modest, Int. J. Heat Mass Transfer 42 (1999) 971.
[43] S.B. Pope, Progress Energy Combust. Sci. 11 (1985) 119.
[44] A. Mbiock, D. Roekaerts, in: Y. Nagano, K. Hanjaliç, T. Tsuji (Eds.), Proceedings of the Third International Symposium on Turbulence, Heat and Mass Transfer, Nagoya, Japan, 2000, p. 873.
[45] http://www.ca.sandia.gov/tdf/Workshop.html
[46] J.H. Frank, R.S. Barlow, C. Lundquist, Proceedings of the Combustion Institute, Vol. 28, The Combustion Institute, Pittsburgh, 2000, p. 447.
[47] Q. Tang, J. Xu, S.B. Pope, Proceedings of the Combustion Institute, Vol. 28, The Combustion Institute, Pittsburgh, 2000, p. 133.
[48] B.E. Launder, in: J.L. Lumley (Ed.), Whither Turbulence? Turbulence at the Crossroads, Springer-Verlag, Berlin, 1990, p. 439.
[49] B.E. Launder, G.J. Reece, W.J. Rodi, J. Fluid Mechanics 68 (1975) 537.
[50] W.P. Jones, in: P. Libby, F. Williams (Eds.), Turbulent Reacting Flows, Academic Press, London, 1994, p. 309.
[51] N. Peters, Twenty-First Symposium (International) on Combustion, The Combustion Institute, Pittsburgh, 1986, p. 1231.
[52] P.J. Coelho, N. Peters, Combust. Flame 124 (2001) 444.
[53] H. Pitsch, M. Chen, N. Peters, Twenty-Seventh Symposium (International) on Combustion, The Combustion Institute, Pittsburgh, 1998, p. 1057.
[54] N. Peters, Progress Energy Combust. Sci. 10 (1984) 319.
[55] W.P. Jones, J.H. Whitelaw, Combust. Flame 48 (1982) 1.
[56] N. Peters, Turbulent combustion, Cambridge University Press, 2000.
[57] K.J. Young, J.B. Moss, Combust. Sci. Tech. 105 (1995) 33.
[58] V. Goutière, A. Charette, L. Kiss, in Proceedings of the Third International Symposium on Radiative Transfer, Antalya, Turkey, 2001.
[59] M.K. Denison, B.W. Webb, J. Heat Transfer 117 (1995) 788.
[60] M.K. Denison, B.W. Webb, J. Quant. Spectrosc. Rad. Transfer 50 (1993) 499.
[61] M.K. Denison, B.W. Webb, Int. J. Heat Mass Transfer 38 (1995) 1813.
[62] M.K. Denison, B.W. Webb, J. Heat Transfer 117 (1995) 359.
[63] P.J. Coelho, Proceedings of the Twelfth International Heat Transfer Conference, Grenoble, France, 2002, p. 705.
[64] W.A. Fiveland, ASME paper 82-HT-20 (1982).
[65] A.S. Jamaluddin, P.J. Smith, Combust. Sci. Tech. 62 (1988) 173.
[66] C.P. Thurghood, A. Pollard, H.A. Becker, J. Heat Transfer 117 (1995) 1068.
[67] R.S. Barlow, J.H. Frank, Twenty-Seventh Symposium (International) on Combustion, The Combustion Institute, Pittsburgh, 1998, p. 1087.
[68] A. Sayre, N. Lallemant, J. Dugué, R. Weber, Twenty-Fifth Symposium (International) on Combustion, The Combustion Institute, Pittsburgh, 1994, p. 235.
[69] Y.R. Sivathanu, J.P. Gore, Combust. Flame 94 (1993) 265.
[70] W.L. Grosshandler, NIST Technical Note 1402, 1993.
[71] C. Ludwig, W. Malkmus, J. Reardon, J. Thomson, Handbook of Infrared Radiation from Combustion Gases, NASA SP-3080, 1973.